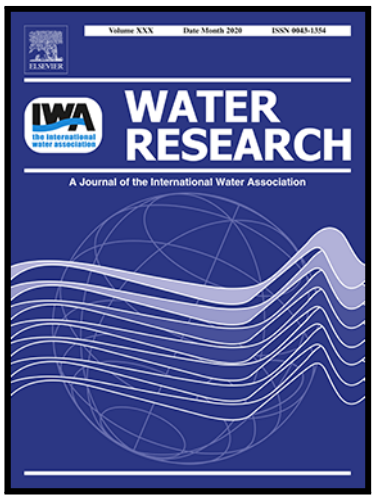

Unravelling winter diatom blooms in temperate lakes using high frequency data and ecological modeling

Xiangzhen Kong , Michael Seewald , Tallent Dadi , Kurt Friese , Chenxi Mi , Bertram Boehrer , Martin Schultze , Karsten Rinke , Tom Shatwell

PII: S0043-1354(20)31216-1
DOI: https://doi.org/10.1016/j.watres.2020.116681
Reference: WR 116681

To appear in: *Water Research*

Received date: 24 July 2020
Revised date: 2 November 2020
Accepted date: 25 November 2020

Please cite this article as: Xiangzhen Kong , Michael Seewald , Tallent Dadi , Kurt Friese , Chenxi Mi , Bertram Boehrer , Martin Schultze , Karsten Rinke , Tom Shatwell , Unravelling winter diatom blooms in temperate lakes using high frequency data and ecological modeling, *Water Research* (2020), doi: https://doi.org/10.1016/j.watres.2020.116681

Highlights

- The winter diatom bloom is studied in a temperate shallow lake fed by groundwater
- High frequency data and lake physical and ecological modeling are employed
- Water temperature and light both regulate diatom growth before the bloom
- Indirect effect of temperature on ice thaw and light condition triggers the bloom
- Silicon limitation and sedimentation terminate the bloom before stratification

Title:

Unravelling winter diatom blooms in temperate lakes using high frequency data and ecological modeling

Authors

Xiangzhen Kong[a,b*], Michael Seewald[a], Tallent Dadi[a], Kurt Friese[a], Chenxi Mi[a], Bertram Boehrer[a], Martin Schultze[a], Karsten Rinke[a], Tom Shatwell[a]

Author affiliations:

[a] UFZ - Helmholtz-Centre for Environmental Research, Department Lake Research, Brückstr. 3a, 39114 Magdeburg, Germany

[b] State Key Laboratory of Lake Science and Environment, Nanjing Institute of Geography & Limnology, Chinese Academy of Sciences, Nanjing, 210008, China

***Corresponding author**: Xiangzhen Kong, **Tel.:** +49 3918109449; **Fax:** +49 3918109150; **Email:** xiangzhen.kong@ufz.de

Abstract

In temperate lakes, it is generally assumed that light rather than temperature constrains phytoplankton growth in winter. Rapid winter warming and increasing observations of winter blooms warrant more investigation of these controls. We investigated the mechanisms regulating a massive winter diatom bloom in a temperate lake. High frequency data and process-based lake modeling demonstrated that phytoplankton growth in winter was dually controlled by light and temperature, rather than by light alone. Water temperature played a further indirect role in initiating the bloom through ice-thaw, which increased light exposure. The bloom was ultimately terminated by silicon limitation and sedimentation. These mechanisms differ from those typically responsible for spring diatom blooms and contributed to the high peak biomass. Our findings show that phytoplankton growth in winter is more sensitive to temperature, and consequently to climate change, than previously assumed. This has implications for nutrient cycling and seasonal succession of lake phytoplankton communities. The present study exemplifies the strength in integrating data analysis with different temporal resolutions and lake modeling. The new lake ecological model serves as an effective tool in analyzing and predicting winter phytoplankton dynamics for temperate lakes.

Keywords: winter diatom bloom; high frequency monitoring; lake modeling; light limitation; temperature

1. Introduction

Diatom blooms have been well-documented in freshwater lake ecosystems (Sorvari et al., 2002; Winder et al., 2008). For eutrophic temperate lakes, a typical seasonal pattern of plankton succession is frequently observed with a spring diatom bloom followed by a summer cyanobacteria bloom (Shatwell and Köhler, 2019; Townsend et al., 1992). These successional stages have been conceptualized in the Plankton Ecology Group (PEG) model (Sommer et al., 2012; Sommer et al., 1986). Winter diatom blooms, however, are under-studied because winter is traditionally considered as an unproductive period.

This concept has recently been challenged, prompting calls to focus more on winter limnology (Hampton et al., 2017). Here we define winter as January to March when the water column in northern temperate lakes is predominantly mixed, and spring as April to June when stratification begins, the same definition as in many other studies (e.g. Shatwell et al., 2019). Understanding lake ecological processes in winter is particularly important because climate change forces faster warming in winter than in other seasons in temperate lakes (Shatwell et al., 2019). It is currently not possible to predict how the anticipated future changes of the global climate during winter will affect seasonal successions. This may constitute a serious source of uncertainty in projecting climate impacts on lake ecosystems, as increasing evidence has shown that biological activities in winter are causally linked with those in the following seasons (Salonen et al., 2009). Potential consequences of shifting winter dynamics include changing nutrient cycling and phytoplankton succession over the year (Wilhelm et al., 2014), uncoupling zooplankton-phytoplankton trophic interactions and phenological mismatch (Winder and Schindler, 2004), or unwanted developments in water quality (Thackeray et al., 2016). To this

end, further investigation of critical winter limnology phenomena and the underlying mechanisms, particularly winter diatom blooms, is timely and essential.

Winter diatom blooms could be driven by a different set of mechanisms from those for spring diatom blooms. Succession of phytoplankton communities are recognized as a consequence of light, water temperature and nutrient limitation (Ferris and Lehman, 2007; Neale et al., 1991; Vincent, 1983; Xiao et al., 2019). Massive diatom developments in winter are reported in many ice-covered lakes with incredible photosynthetic efficiency due to a stable water column and inverse stratification (D'souza et al., 2013; Reavie et al., 2016; Spaulding and Baron, 1993). In temperate stratified lakes, light is considered to be the sole limiting factor in winter and early spring (Sommer et al., 1986). The onset of stratification is considered as a 'light switch' enabling net phytoplankton growth at a time when nutrients are sufficiently high and grazers are not yet present in significant abundances, and initiating the spring bloom. The emerging grazers, parasitism and pathogens in late spring are usually considered as the terminators of spring diatom blooms (Sommer et al., 2012). Regarding winter diatom blooms, however, the classic 'light switch' does not play a role because such blooms usually start before the onset of stratification. Whereas ice thaw was proposed as the major trigger of such blooms in shallower lakes (Shatwell et al., 2008), a complex interaction between factors of temperature, light and nutrients may also contribute to the mass development of diatoms (Nicklisch et al., 2008). Further, little is known about the bloom terminator, which could be sedimentation resulting from the onset of stratification or nutrient limitation (Goto et al., 2007; Thackeray et al., 2008). Thus, we can hypothesize that the role of stratification onset in driving the diatom growth depends on the timing of the bloom. Early diatom blooms that occur at the end of winter during deep recirculation can be terminated by stratification onset due to enhanced water column

stability and diatom sedimentation. On the other hand, later blooms that occur in spring can be triggered by stratification onset, which enhances the light conditions for organisms in the epilimnion. Finally, contrasting evidence prevails regarding the dominant species either as large (e.g. *Aulacoseria granulata*) (Yang et al., 2016) or small centric species (e.g. *Stephanodiscus neoastraea*) (Kirilova et al., 2008; Shatwell et al., 2008). Taken together, factors determining the timing, dynamics, and composition of winter diatom blooms remain far from conclusive and require quantitative investigations.

Several challenges constrain further research. Sampling during winter is often complicated due to ice cover and thus less frequent. The temporal frequency of regular sampling (e.g. monthly) is insufficient to capture the dynamics of algal blooms and their driving factors in detail. In addition, simultaneous monitoring of meteorology, lake physical characteristics and water quality profiles are generally scarce. Even with sufficient data, reliable predictions of winter phytoplankton dynamics for a given inland aquatic system remain challenging. Exploiting a combination of *in situ* high frequency monitoring techniques and process-based lake modeling techniques may shed more light on winter limnology as has been successfully demonstrated in other applications in limnology (Kong et al., 2019).

To address these questions, we investigated a temperate freshwater lake (Lake Barleber) in central Germany with intermediate depth (mean 6.7 m) and hyper-eutrophic state, which underwent a massive diatom bloom in winter 2019. Our hypotheses are: 1) rather than a single trigger of light, both water temperature and light interactively drive the winter diatom bloom; 2) the bloom is terminated by silicon limitation and sedimentation near the onset of lake stratification; and 3) the winter diatom bloom is dominated by small centric species rather than larger pennate or colonial diatoms. We synthesized and analyzed data across one year from

multiple sources, including *in situ* high frequency monitoring, meteorological databases, and biweekly sampling of water quality variables. In addition, we developed an ecological model including competition between three phytoplankton species typically dominating lowland hyper-eutrophic German lakes in spring (one small solitary centric diatom, one pennate diatom, and one cyanobacterium). Even though the pennate diatom is better adapted to low light, we expect that the small centric diatom outcompetes the other two species during the simulation because it is best adapted to low temperature. The comprehensive dataset facilitated modeling lake physical and ecological dynamics and unraveled mechanisms driving this bloom event, which were found different from those for spring diatom blooms.

2. Materials and methods

2.1 Study site

Lake Barleber is located in the city of Magdeburg, Germany (52°13’15’’ N, 11°39’0’’E) (Fig. 1). The lake was formed by gravel excavations at the beginning of the 1930s, with a surface area of approximately 1 km^2, a maximum depth of 11.0 m and an average depth of 6.7 m. The lake is monomictic as it is stably stratified in summer, while mixed in other seasons (except for short ice cover periods when the lake is temporarily inversely stratified). There is no surface in- or outflow: the lake is fed only by groundwater and precipitation. With an annual groundwater inflow of 640,000 m^3, water residence time is approximately 10 years (Hannappel and Strom, 2020). It was initially dominated by macrophytes but became progressively eutrophic and dominated by phytoplankton due to release of sediment-borne phosphorus (P). In 1986, a lake-wide phosphorus removal with an aluminum addition turned the lake back into the mesotrophic

132 state with a diverse macrophyte community (Klapper and Geller, 2001), but since 2016 the lake
133 again switched into an eutrophic state.
134
135 ***2.2 Sampling schemes and data preparation***
136 The main sampling site was BA1 (Fig. 1), where water samples were collected at five
137 depths (0.5, 2.5, 5.0, 7.0 and 9.0 m), and water temperature profiles were measured with manual
138 probes (Table S1). The sampling frequency varied from weekly during warm seasons (Jun.-Sep.
139 2018, and Mar.-Jul. 2019; every second day during the cyanobacteria bloom in July 2018) to
140 biweekly/monthly during cold seasons (Oct. 2018-Feb. 2019). Water chemistry variables (total
141 nitrogen (TN), nitrate nitrogen (NO_3-N), ammonium nitrogen (NH_4-N), total phosphorus (TP),
142 soluble reactive phosphorus (SRP) and silicon (Si) concentrations) were measured in the
143 laboratory using standard methods (Table S1). Volume-weighted concentrations were calculated
144 for the whole water column during mixing, and separately for the epilimnion and hypolimnion
145 during the stratified period. Secchi depth (z_{secchi}) was measured manually using a Secchi disk. In
146 addition, the thermistor chain captured water temperatures at 15 depths (Table S1) every 15
147 minutes. Moreover, we used a multi-parameter probe to manually capture vertical profiles of
148 temperature, electrical conductivity, salinity, pH, turbidity, oxygen, and chlorophyll-a
149 fluorescence, and a multi-channel fluorescence probe to determine the phytoplankton
150 composition in terms of specific chlorophyll-fluorescence from diatoms, green algae,
151 cryptophytes, and cyanophytes (Beutler et al., 2002). Water chemistry and probe data were all
152 linearly interpolated from 0.0 m to 9.0 m at 0.5 m intervals and then linearly interpolated to daily
153 resolution. In addition, we collected phytoplankton samples and fixed them with Lugol's solution

154 during the diatom bloom (Mar. 4th, 2019) and observed the samples under an inverted
155 microscope to identify the dominant phytoplankton group.
156 In addition to manual sampling and profiles, a high frequency monitoring buoy measured
157 near-surface water conditions every 10 minutes at the BAM site in the middle of the lake (Fig. 1
158 and Table S1). A multi-parameter probe and a multi-channel fluorescence probe were both
159 integrated into the buoy system and permanently suspended at 0.5 m depth for continuous
160 monitoring of physic-chemical properties (temperature, conductivity, pH, turbidity, oxygen, and
161 chlorophyll-a concentration) and phytoplankton community dynamics in the surface water. All
162 high frequency datasets were further aggregated to daily intervals.
163 We collected meteorological data from the German meteorology service (DWD) via the
164 R package 'rdwd' (Boessenkool, 2019) at the station 'Magdeburg' (ca. 15 km south from the
165 lake), including air temperature (°C), air pressure (hPa), humidity (%), mean wind speed ($m \cdot s^{-1}$)
166 and precipitation (mm, including snow) at hourly interval, and sum of solar incoming radiation
167 ($J \cdot cm^{-2}$) for every 10 minutes (Fig. S1). Solar radiation was aggregated to hourly intervals. In
168 addition, we obtained historical climate data at station 'Magdeburg' from 2010 at 10 minutes
169 resolution.
170
171 ***2.3 Statistics***
172 During the deep circulation period (October 2018 to March 2019), we tested the
173 differences of the volume-weighted nutrient concentrations before and after the onset of the
174 winter diatom bloom. We applied a generalized least squares (GLS) model with a first-order
175 autoregressive correlation structure (AR(1)) to analyze the nutrient time series data against a
176 binary variable as the proxy of the winter diatom bloom (0: no bloom; 1: bloom). The GLS

177 model was implemented in R (R Core Team, 2018) using the function 'gls' in package 'nlme'
178 (Pinheiro et al., 2012).
179
180 ***2.4 Physical characteristics evaluation***
181 Water surface temperature was estimated as the mean value in the upper 1 m layer (at 0.0
182 and 1.0 m depth), and bottom temperature as the mean value measured at 6.5 and 7.5 m around
183 the mean depth (6.7 m). The onset and end of lake stratification was considered as start and end
184 of the longest period in the year with a temperature difference higher than 1°C between the
185 surface and bottom (Shatwell and Köhler, 2019). Thermocline depth during the stratification was
186 calculated using the function 'ts.thermo.depth' in package 'rLakeAnalyzer' (Winslow et al.,
187 2019) in R (R Core Team, 2018). The mixed layer depth (h, m) was assumed to be the mean lake
188 depth when the lake was isothermal, and the thermocline depth when the lake was stratified
189 (Shatwell and Köhler, 2019). z_{secchi} was linearly interpolated over time between measurements to
190 the daily scale, and the light extinction coefficient (ε, m^{-1}) was calculated from z_{secchi} as: ε =
191 $2.05/z_{secchi}$, obtained from similar waterbodies in Germany (Shatwell et al., 2016). The mean
192 daily underwater light intensity (I_m, $mol \cdot m^{-2} \cdot d^{-1}$) in the mixed layer (down to depth of h) was
193 calculated based on the Lambert-Beer law: $I_m = I_0(\varepsilon h)^{-1}(1 - e^{-\varepsilon h})$, where I_0 was the
194 photosynthetically available radiation (PAR) just below the water surface. I_0 was estimated from
195 daily solar radiation, assuming 4.56 μmol photons$\cdot J^{-1}$, PAR proportion within solar radiation of
196 50%, and 10% reflection and backscattering at the water surface (Shatwell and Köhler, 2019).
197 During the ice cover period (Jan. 14th-Feb. 4th 2019), I_0 was reduced by 50% as an empirical
198 estimation (Kirillin et al., 2012). We assumed a value of 1.3 (0.8-2.5) $mol \cdot m^{-2} \cdot d^{-1}$ as the critical
199 light intensity for positive net growth of phytoplankton (Köhler et al., 2018; Siegel et al., 2002;

Sommer and Lengfellner, 2008). The effective photoperiod was calculated as the length of the solar day multiplied by the ratio of euphotic to mixed depth ($z_{eu}\ z_{mix}^{-1}$) when $z_{eu}\ z_{mix}^{-1} < 1$, to account for periods when phytoplankton are in effective darkness below the euphotic layer; z_{eu} was considered to be the depth of 1% of surface light, given by $z_{eu} = -\ln(0.01)\ \varepsilon^{-1}$.

2.5 Modeling

Two modeling approaches were implemented in this study. The first was estimating the period of ice cover and thickness from November 2018 to April 2019 using the one-dimensional bulk hydrodynamic model FLake, a process-based model to simulate lake thermal regimes (Kirillin et al., 2011; Mironov, 2008). The model consists of two water layers representing the simplified vertical structure of the water column including the ice cover (Shatwell et al., 2019). FLake has been widely used especially in numerical weather prediction and climate research, and is readily applicable for lakes with different conditions (Kirillin et al., 2017; Shatwell et al., 2019; Thiery et al., 2014). Model inputs included air temperature (°C), vapor pressure (mb), wind speed ($m \cdot s^{-1}$), cloud cover (-) and solar incoming radiation ($W \cdot m^{-2}$), obtained from the DWD described above. Vapor pressure was calculated as the product of saturated vapor pressure (calculated from air temperature, according to Tabata (1973)) and relative humidity.

The second approach aimed at simulating phytoplankton dynamics during the winter diatom bloom to elucidate the underlying mechanisms. A lake ecological model (Fig. 2) was developed to simulate phytoplankton growth and the competition between species that typically dominate lowland hyper-eutrophic German lakes in spring. The model is zero-dimensional and is valid for a mixed water column or water layer. The state variables in the model include P and Si both dissolved in water and stored in sediment, biovolume of two diatoms (*Stephanodiscus*

minutulus and *Nitzschia acicularis*) and one cyanobacterium (*Limnothrix redekei*), as well as the biovolume quota of P within each species of algae. The model assumed a constant fraction of Si in the two diatom species as observed in experimental data. *S. minutulus* is a centric diatom usually dominating in early spring, which is a strong competitor for Si, a low temperature, short-photoperiod specialist and specially adapted to early spring conditions. *N. acicularis* is a late spring pennate diatom, a P-specialist, and grows rapidly under optimal conditions. *L. redekei* is a late spring cyanobacterium, which grows much slower than both diatoms, but is a superior competitor under P-limitation (Nicklisch, 1999) and has no Si requirements. All three species are well adapted to low light conditions, with a low light compensation point and high light use efficiency (see Table S2) compared to other common species (Reynolds, 2006). The model accounted for the species-specific 3-way interactions between temperature, photoperiod and the respective limiting resources (light, phosphorus and silicon). It could thus determine e.g. the relative contribution of different factors in constraining growth rates. Model parameters related to growth kinetics, light absorption, nutrient and chlorophyll content were calculated directly from culture experimental data at high accuracy (Foy, 1983; Gibson and Foy, 1983; Kohl and Giersdorf, 1991; Nicklisch, 1992; Nicklisch and Kohl, 1989; Nicklisch et al., 1991; Shatwell et al., 2013; Shatwell et al., 2014; Shatwell et al., 2012) (Table S2 and S3). Inputs to the model include mean light availability, water temperature, effective photoperiod and mixed layer depth, all at daily intervals during the simulation period (Jan. 1st to Mar. 31st, 2019). The model is written in R (R Core Team, 2018) and solved using the package 'deSolve' (Soetaert et al., 2010). Details of the model are explicitly described in the supporting information (SI Text).

3. Results

3.1 Occurrence of the winter diatom bloom

We observed a massive algal bloom during Feb. and Mar. 2019, with a maximum chlorophyll concentration up to 93.4 $\mu g \cdot L^{-1}$ on Mar. 1st (Fig. 3). While the Chlorophyll-a fluorescence was unable to distinguish diatoms and dinoflagellates, microscopic inspections revealed that the massive winter algal bloom consisted of small centric diatoms while dinoflagellates were not present. On the contrary, dinoflagellates were present at high abundance and diatoms were almost absent during summer 2018. The winter diatom bloom reached a concentration that was approximately 1.4 times higher than that in the previous summer when cyanobacteria and dinoflagellates bloomed together (maximum 68.4 $\mu g \cdot L^{-1}$ on September 4th, 2018). Chlorophyll-a fluorescence data from profiles during regular sampling confirmed the occurrence of the winter diatom bloom in 2019, and further revealed that the diatoms were homogeneously distributed in the water column during the bloom (Fig. S2). We considered the first day of the exponential growth of diatoms as the start of the diatom bloom (Feb. 5th) (Fig. 4a), and the day with the minimum value before the spring algal development as the end (Mar. 20th) (Fig. 3a). There were several short-term diatom developments during Jan. 24th to Feb. 4th 2019 before the bloom started (Fig. 4a).

3.2 Meteorological and lake physical conditions

Lake Barleber was ice covered from Jan. 14th to Feb. 4th, 2019 just before the winter bloom (approximately two thirds of the surface area). Measured data showed that water temperature started to decline from the start of ice cover throughout the water column, following the decline in air temperature that fell below zero (Fig. 4b). Water temperatures from the surface to the bottom were below 4°C and demonstrated intermittent inverse stratification from Jan. 15th

to Feb. 4th (Fig. 3c). The inverse stratification was transient and restricted to the upper 1 m of the water column, suggesting incomplete ice cover with changing ice thickness and coverage area over time. This inference was further supported by predictions of ice thickness from the 1D hydrodynamic model FLake (Fig. 4c and S3). The model indicated two periods with ice cover on the lake, one at the end of January and the other at the beginning of February, with an ice thickness up to 0.7 cm. This is an estimation of the average ice thickness across the lake surface without considering the spatial heterogeneity. In addition, there was frequent snowfall during the ice cover period (Fig. 4c) that could have profound effects on light under ice. Taken together, we concluded that the lake was at least partially covered by ice during Jan. 14th to Feb. 4th, 2019, with relatively low ice thickness. It is thus reasonable to reduce the light below water surface during ice cover by a factor of 0.5 to calculate the mean water column light intensity (I_m) (Fig. 4d).

The diatom bloom started immediately after ice thaw, in parallel with changes in lake physical conditions including an increase in air and water temperature, light intensity, termination of inverse stratification and onset of deep recirculation (Fig. 3 and 4). The lake was well-mixed and isothermal during the diatom bloom except for short-term heating and cooling on the surface (Fig. 3c) and stratification started soon after the diatom bloom collapsed (Fig. 3b). Furthermore, light intensity fluctuated around the critical value of 1.3 mol·m^{2}·day^{-1} before the onset of the diatom bloom (Fig. 4d) and stayed mostly above the critical value afterwards.

3.3 Water quality

The lake was hyper-eutrophic due to high TP concentrations (mean 0.42 mg·L^{-1} with a range of 0.05-0.71 mg·L^{-1}) during the study period (June 2018 to June 2019). The system was P-

limited in winter with dissolved inorganic nitrogen (DIN):total phosphorus (TP) ratios of 2.3 to 3.1 (1.6 as the threshold; Dolman et al., 2016). Except for NO_3-N, concentrations of other nutrients were all significantly lower after the onset of the diatom bloom ($p<0.05$) (Table 1, Fig. S4). Data for Si concentrations were not directly available before the onset of the diatom bloom, but Si concentration in the previous November sampling reached 1.55 $mg \cdot L^{-1}$. After the bloom, Si decreased to 0.05 $mg \cdot L^{-1}$ close to the detection limit (0.02 $mg \cdot L^{-1}$). The decline was also pronounced for SRP (from 337 to 242 $\mu g \cdot L^{-1}$) and ammonium (from 0.76 to 0.17 $mg \cdot L^{-1}$). Furthermore, we observed changes in multiple water quality variables in parallel with the diatom bloom (Fig. S5). Oxygen level increased rapidly to a maximum concentration of 23.1 $mg \cdot L^{-1}$ and saturation of 182.5% in the middle of the bloom. Meanwhile, there was an increase in pH throughout the water column (8.41-9.13) pointing to high photosynthetic activity.

3.4 Ecological modeling

Model predictions of nutrients and various water quality proxies fit nicely to the field observations, with low root mean-square error (*RMSE*) and high correlation coefficient (*r*) values (Fig. 5). The model predicted that rather than large pennate diatoms (*N. acicularis*) and cyanobacteria (*L. redekei*), small centric diatoms, as represented by *S. minutulus*, would dominate the phytoplankton community during the bloom (Fig. 6a), which was also consistent with observations. Dissolved P in the model prediction was consumed rapidly during the bloom but was not shown in the observations, implying that the model might have underestimated relevant processes for P cycling, such as sediment mineralization and release. The model clearly showed that abrupt silicon limitation and subsequent sedimentation losses terminated the bloom.

The model further indicated that rather than a single trigger of light, an increase of both water temperature and light intensity interactively initiated the diatom bloom (Fig. 6b). Before the bloom, constraint mainly by temperature and light together reduced the net growth rate of *S. minutulus* from the maximum 1.3 d^{-1} to a level fluctuating around zero. Fluctuations of net growth rate on certain days were most likely attributed to cloudiness (as shown in Fig. S1c for global radiation). Then, a period with continuous positive net growth rate initiated the diatom bloom, implying that constraints from temperature and light intensity were both weakened. Effective photoperiod showed little effect except for the period with the peak diatom biomass (beginning of March). After the biomass peak, limitation by Si depletion became dominant and drove the bloom to the end (inner panel of Fig. 6b). Our model therefore revealed a complex interplay of factors including temperature, light and nutrients in driving the winter diatom bloom.

4. Discussion

4.1 Mechanisms of the winter diatom bloom

Both our analyses of field data and modeling outcomes suggest different mechanisms for driving the diatom blooms in winter than in spring. Winter diatom assemblages under ice-covered lakes are primarily driven by high photosynthetic efficiency and a stable water column (D'souza et al., 2013; Spaulding and Baron, 1993). Besides, light is particularly emphasized in the PEG model as the key factor triggering the spring phytoplankton buildup, following the concept of critical mixing depth (Sverdrup, 1953). The onset of stratification in deeper lakes (>30m in depth) typically brings an order-of-magnitude increase in light availability, serving as a 'light switch' of the diatom bloom (Sommer et al., 2012). In shallower lakes, the spring bloom can begin before the onset of thermal stratification during the winter circulation period, when

337 lakes are typically mixed to the bottom. In addition, the revised version of the PEG model
338 specifically states that temperature is unimportant for winter phytoplankton dynamics (Sommer
339 et al., 2012). This is based on the fact that dominant algal species in winter are usually well
340 adapted to cold conditions. In addition, experimental studies show that water temperature has
341 little effect on the initial slope of algal growth-light and photosynthesis-light curves under low
342 light conditions (Davison, 1991; Foy, 1983; Talling, 1957), because photochemical rather than
343 enzymatic processes are rate limiting. This has led to the view that temperature is unimportant,
344 but this conclusion neglects the interaction between temperature and light. Low temperatures
345 decrease the threshold at which light becomes limiting (Nicklisch et al., 2008), so that light may
346 be close to growth-saturating even at the low intensities that occur in winter in temperate lakes.
347 The interaction therefore increases the relative importance of temperature. Accordingly, higher
348 growth rates can only be achieved by simultaneously increasing light and temperature, and thus
349 both factors must be considered as co-limiting. Here we define 'limiting' in terms of growth rates
350 rather than in terms of biomass, which can only be limited by true resources like light and
351 nutrients.

352 Based on the modeling, which disentangled the individual effects of temperature and
353 light, we found that both factors are important to the diatom bloom and the bloom was most
354 likely initiated by a complex interaction of them (Fig. 6b). We further supported this finding by
355 projecting the observed water temperatures and light values during the bloom over the isoclines
356 of equal specific growth rate (at 0.2 d^{-1} as a typical value during the bloom) estimated by the
357 model (Fig. 7a). We found that the points showing the water temperature and light intensity in
358 the water column during Jan. 1st and Mar. 20th, 2019 were distributed along both limbs of the
359 isoclines, suggesting constraints from both factors. The isocline for *S. minutulus* is closest to the

origin around the points, showing that this species can achieve the same growth rate as the other species at lower light and temperature. This reflects its specific adaptation to these conditions and explains why this species dominates in the model during the cold periods.

In addition, specifically for *S. minutulus*, we compared the relative strength of the growth constraint by both light energy and temperature before and during the bloom using the constraint vector $\left(\frac{\partial \mu}{\partial I}, \frac{\partial \mu}{\partial T}\right)$ (Fig. 7b) based on the model estimations (Fig. 7c-e). We found that the arrows representing the constraint vector demonstrated both vertical and horizontal directions (Fig. 7b), implying that both factors played a role in driving the diatom bloom. This method further categorized the light and temperature condition field into either 'light-constraint' or 'temperature-constraint'. Accordingly, light and temperature alternatively acted as the major constraint on the growth of *S. minutulus* before the onset of the bloom (Fig. 6b). Then, at the exponential growth stage of the diatom, temperature constrained the growth on most days, as an increase in temperature would have brought a greater increase in growth rate of *S. minutulus* than an increase in light. This is evident for conditions where the arrows are almost vertical, showing that light energy plays a minor role. Interestingly, light was strongly constraining only on some overcast days, as shown by arrows with a large horizontal component.

We further proposed that water temperature contributed to the onset of the winter diatom bloom both directly and indirectly. The direct effects were physiological and allowed higher growth rates of diatoms (Fig. 6b). The indirect effects included driving the ice thaw and water mixing, which were likely more pronounced. The lake became fully mixed after ice thaw, allowing for rapid increase in both light intensity and water temperature. Growth limitation on the diatoms was therefore weakened, which initiated exponential growth. Our results therefore highlight the fundamental role of water temperature in driving winter diatom blooms, which can

383 be considered as an auxiliary 'switch'. Altogether, the physical environment is important for the
384 onset of winter diatom bloom rather than simply the amount of light.

385 We found that nutrients were not limiting at the beginning of the bloom, but Si limitation
386 ultimately terminated the bloom. This was indicated by both nutrient data (Fig. S4) and the
387 modeling results (Fig. 6b). Though ammonium was also almost depleted at the end the bloom,
388 diatoms may use nitrate as an alternative nitrogen source for growth, so that the bloom was
389 unlikely terminated by N limitation. Moreover, SRP concentrations during the bloom were too
390 high (>200 $\mu g \cdot L^{-1}$) to indicate P limitation of phytoplankton. Results from an experimental study
391 (Shatwell et al., 2013) implied that the initial Si concentration of ~1.5 $mg \cdot L^{-1}$ would be far above
392 the range for Si limited growth of both diatom species before the diatom bloom. The apparent
393 half-saturation constant in the Monod model of specific growth rates was about 0.025 and 0.046
394 $mg \cdot L^{-1}$ for *S. minutulus* and *N. acicularis*, respectively, across various conditions of temperature
395 (5-20°C) and photoperiod (6-12 $h \cdot d^{-1}$). The reduction of the Si concentration from ~1.5 to ~0.05
396 $mg \cdot L^{-1}$ fully complied with the increase of diatom biomass, and also suggested limitation by Si
397 (Fig. 6b). Mostly, the emergence of grazers (Köhler et al., 2005; Lampert et al., 1986; Sommer et
398 al., 2012), or parasitism, particularly by chytrids (Frenken et al., 2017; Ibelings et al., 2011) are
399 responsible for terminating spring diatom blooms. Though we cannot exclude these factors
400 (because we did neither observe nor model the abundance of grazers or chytrids), we assume that
401 silicon limitation and sedimentation played the major role. The onset of silicon limitation is
402 usually abrupt and recycling is slow at low temperature. If there is no external supply of fresh
403 silicon, the diatom biomass can no longer increase and the bloom is inevitably terminated. The
404 model suggested that the bloom dynamics could be explained entirely by abiotic factors, and that
405 diatoms grew exponentially during the bloom as in a batch culture without signals of grazing

406 (Fig. 6a). Si limitation was apparently predominating in the end of the bloom (Fig. 6b). In fact,
407 we think the absence of significant losses due to grazing or parasitism facilitated the high peak
408 biomass close to the limit set by complete incorporation of available silicon. Previous studies
409 also demonstrate that grazing pressure decreases and Si limitation increases when diatom blooms
410 occur earlier, for instance due to climate warming (Shatwell et al., 2008; Thackeray et al., 2008;
411 Winder and Schindler, 2004).
412
413 ***4.2 Composition of the diatom bloom***
414 We observed that small centric species similar to *Stephanodiscus* spp. dominated the
415 winter diatom bloom in Lake Barleber. Modeling results also suggest that *Stephanodiscus* spp.
416 may outcompete other species (e.g. *N. acicularis*) in winter (Fig. 6a). This finding is against our
417 expectation that winter diatom blooms are typically dominated by large diatoms such as
418 *Aulacoseria* spp., as observed in many other lake systems (Horn et al., 2011; Yang et al., 2016).
419 These large species display a combination of traits that mediate high competitive abilities,
420 including low-light and low temperature adaptation, accumulation of nutrient reserves, and
421 strong benthic-pelagic coupling that allow them to form a considerable winter inoculum in deep
422 water (Jewson et al., 2010; Lewandowska et al., 2015). Winter inoculum is the key for the
423 domination of large diatoms because in this way they can establish priority and build up nutrient
424 reserves to outcompete other species (Gibson, 1981; Padisák et al., 2003). However, in Lake
425 Barleber, nutrients (particularly P) were abundant and the nutrient storage capabilities of large
426 rather slow-growing diatom species like *Aulacoseira* spp. may not provide a significant
427 advantage. Moreover, small, fast growing species such as *Stephanodiscus* spp. are probably
428 stronger competitors under Si limitation (Kilham et al., 1986; Shatwell et al., 2013). In addition,

429 a sensitivity analysis of the model to the sinking velocity (assigned to 0.1, 0.3 and 0.5 $m \cdot d^{-1}$) of
430 the two diatom species (*S. minutulus* and *N. acicularis*) demonstrated marginal effects of sinking
431 velocity on the ecological dynamics during winter 2019 in Lake Barleber (Fig. S6), implying that
432 the dominance of *S. minutulus* was attributed more to the other competitive advantages such as
433 Si uptake and adaptation to low photoperiod. It is noteworthy that diatom blooms dominated by
434 *Stephanodiscus* spp. in mild winters were also observed in the polymictic and eutrophic Lake
435 Müggelsee (Berlin, Germany) with a mean depth of 4.9 m (Shatwell et al., 2008). Taken together,
436 in hypereutrophic lakes with shallow to intermediate depth such as Lake Barleber, the winter
437 diatom assemblage is more likely dominated by small, centric species.
438
439 ***4.3 Merits and limitations of the methodology***
440 We demonstrate high resolution monitoring as an effective tool to refine the recognition
441 of limnological phenomena and to unravel new mechanisms. The high frequency data on water
442 temperature profiles, water quality and phytoplankton community provide a unique opportunity
443 to investigate the comprehensive picture of the short-term winter phytoplankton dynamics and to
444 evaluate the underlying mechanisms in detail. This would be difficult with the data from regular
445 sampling at a biweekly resolution or coarser during cold seasons. Furthermore, we showcase the
446 strength of combining high frequency data with those from regular monitoring, as high frequency
447 data cover a fine temporal resolution of a small set of target variables, while regular sampling
448 data include a more comprehensive set of variables but at a relatively low frequency.
449 Our dataset inevitably contains gaps (e.g. missing ice data and Si concentrations before
450 the bloom). We performed a dual modeling approach to compensate for such weakness and to
451 provide more insights on the mechanisms driving the diatom bloom. Agreement between the

model outputs and the observations were primarily attributable to the following reasons. First, the model configuration represented the majority of physical and ecological components and processes in the lake that were critical during the winter diatom bloom. The ecological model explicitly considered a well-chosen functional diatom group dominating in the field, and the species-specific interactions between growth factors (light, temperature, photoperiod, and nutrients). Second, all growth parameters for light-, P-, Si-, temperature-, and photoperiod-constraint growth were directly measured in laboratory experiments for all species (Table S2) rather than calibrated or estimated, representing a high degree of realism. Third, the models were driven by high quality external forcing data including *in situ* measurements of in-lake physical and chemical conditions. Altogether, the models in the present study were capable of reproducing the dynamics of key processes in the lake, so that their predictions of those variables without observations (ice thickness and Si concentrations) could be relied on. We therefore see the potential to apply these models as ecological forecasting tools, e.g. with respect to the occurrence of diatom blooms in temperate lakes. Nevertheless, we explicitly focus on winter ecological dynamics so that some processes in the ecological model (such as nutrient release from sediment and maximum phosphorus uptake rate) are not temperature dependent for simplicity. These processes should be coupled to temperature if the model is applied during periods with larger temperature variation or when Si:P ratios are higher, which would be an important step forward for the model improvement in the future.

4.4 Implications and perspectives

Our findings for winter diatom blooms would be relevant to other gravel pit and groundwater-fed lakes, which are globally widespread due to the high demand of gravel and sand

475 (1.7×10^8 metric tons per year) for construction (Mollema and Antonellini, 2016). In addition, our
476 results may also apply to temperate, shallow to medium depth lakes and reservoirs in general fed
477 by surface inflows which supports the phenomenon of diatom growth in winter. We further
478 applied the developed ecological model to Lake Müggelsee (natural, temperate riverine lake,
479 mean depth 4.9m, fed by Spree river, retention time 6 weeks), which also supports winter blooms
480 of small centric diatoms (Shatwell et al., 2008). The good model results (Fig. S7) illustrate the
481 general applicability of our findings because the principles in the model about the interactive
482 effects of light and temperature are universal. Further, such winter diatom blooms can occur in
483 oligo- and mesotrophic lakes (Goto et al., 2007) and drinking water reservoirs (Horn et al., 2011),
484 provided they are not too deep. However, the species dominating these blooms, and thus their
485 dynamics, may differ from the more eutrophic species modeled here. Deep drinking water
486 reservoirs usually experience typical spring diatom blooms (Horn et al., 2015; Wentzky et al.,
487 2019). Altogether, we infer that our results apply in general to temperate, eutrophic, shallow to
488 moderately deep lakes that can experience mild winters or intermittent ice cover.

489 Our findings can be valuable for evaluating the impact of climate change on inland
490 freshwater ecosystems. With increasing air temperature in a future climate, model projections
491 demonstrate higher surface water temperature, thereby reducing ice cover and extending the
492 circulation period before stratification for lakes (Shatwell et al., 2019; Woolway and Merchant,
493 2019). Given the important role of water temperature shown here, we expect more frequent
494 winter diatom blooms in Lake Barleber and also in similar temperate lakes. In addition, the
495 intensity of the diatom bloom could be larger because previous studies have shown that the
496 bloom intensity correlates with the duration of the circulation period (Horn et al., 2011).
497 Furthermore, earlier ice thaw results in lower temperature for diatom growth, which may shift

498 the diatom composition from large pennate to small cold-adapted centric species as we found
499 here in Lake Barleber. The dominance of highly edible small centric diatoms (rather than their
500 large, less edible counterparts) was likely to impose knock-on effects on the earlier occurrence of
501 zooplankton, which possibly altered the seasonal succession of plankton communities. The
502 consequences of changing patterns of winter diatom blooms on the lake ecosystem structure and
503 functioning are subject to further investigations.
504

505 ## 5. Conclusions

506 Ecological dynamics of temperate lakes in winter are poorly understood because winter
507 was long thought to be dormant, and was consequently ignored in most sampling campaigns. We
508 examined the occurrence and short-term dynamics of a massive winter bloom of diatoms in a
509 German lake, which exceeded the annual biomass maximum of the previous year. The results
510 showed that this bloom was dominated by small centric diatom species rather than their larger
511 counterparts. We demonstrate that temperature can no longer be ignored in winter dynamics, but
512 that both temperature and light are decisive. We therefore challenge the current paradigm of sole
513 control by light availability on lake phytoplankton growth in winter. Our new findings were
514 attributed to the combination of regular field sampling, *in situ* high-frequency monitoring, and
515 modeling of the lake. We provide a novel model of the species-specific interactive effects of
516 different factors on algal dynamics. The model parameters are based on a large set of
517 phytoplankton bioassay data and was implemented without calibration, so as to give a high
518 degree of realism and become applicable to temperate lakes in general. Overall, increasing
519 frequency of winter biological activities in lakes such as diatom blooms are inevitable in the

context of climate change, calling for more insights on the lake winter limnology and their implications on the seasonal succession of biogeochemical and ecological processes.

Acknowledgments

We thank our colleagues in the Lake Research department at Helmholtz-Centre for Environmental Research (UFZ) for helpful discussions on the manuscript. We thank our UFZ colleagues Karsten Rahn and Martin Wieprecht who performed the field sampling in Lake Barleber, Burkhard Kuehn for maintaining the buoy, the UFZ Analytics Department (GEWANA) for performing the chemical analysis of the collected samples, and we thank Peter K. Friz for advice on Fig. 7. We also thank the editor and three anonymous reviewers who provided constructive comments and suggestions to improve the manuscript. The monitoring of Lake Barleber was partially funded by the Helmholtz Association in the framework of Modular Observation Solutions for Earth Systems (MOSES) and the city of Magdeburg. X. Kong is supported by a postdoctoral fellowship from the Alexander von Humboldt Foundation in Germany. This study was also partially funded by the National Key Research and Development Program of China (2019YFA0607100) and the Deutsche Forschungsgemeinschaft (DFG, German Research Foundation) within the project DIABLO under grant - SH 915/1-1.

Notes

The authors declare no conflict of interest. Upon acceptance, the data and the R script for the ecological model supporting the results in this manuscript will be archived and made publicly available at a proper online repository. The R script can be used for testing and evaluating the

ecological model developed in the present study. The repository DOI will be included at the end of the article.

Supplementary materials

Additional information include: SI Text for description of the ecological model, SI Figures S1-S7, and SI Tables S1-S3.

Reference

Beutler, M., Wiltshire, K.H., Meyer, B., Moldaenke, C., Lüring, C., Meyerhöfer, M., Hansen, U.-P. and Dau, H. 2002. A fluorometric method for the differentiation of algal populations in vivo and in situ. Photosynth. Res. 72(1), 39-53.

Boessenkool, B. 2019. rdwd: Select and Download Climate Data from 'DWD' (German Weather Service). R package version 1.2.0. https://CRAN.R-project.org/package=rdwd.

D'souza, N., Kawarasaki, Y., Gantz, J., Lee, R., Beall, B., Shtarkman, Y., Kocer, Z., Rogers, S., Wildschutte, H. and Bullerjahn, G. 2013. Diatom assemblages promote ice formation in large lakes. ISME J. 7(8), 1632-1640.

Davison, I.R. 1991. Environmental effects on algal photosynthesis: temperature. J. Phycol. 27(1), 2-8.

Dolman, A.M., Mischke, U. and Wiedner, C. 2016. Lake‐type‐specific seasonal patterns of nutrient limitation in German lakes, with target nitrogen and phosphorus concentrations for good ecological status. Freshwat. Biol. 61(4), 444-456.

563 Ferris, J.A. and Lehman, J.T. 2007. Interannual variation in diatom bloom dynamics: roles of
564 hydrology, nutrient limitation, sinking, and whole lake manipulation. Water Res. 41(12),
565 2551-2562.
566 Foy, R.H. 1983. Interaction of temperature and light on the growth rates of two planktonic
567 *Oscillatoria* species under a short photoperiod regime. Br. Phyco. J. 18(3), 267-273.
568 Frenken, T., Alacid, E., Berger, S.A., Bourne, E.C., Gerphagnon, M., Grossart, H.P., Gsell, A.S.,
569 Ibelings, B.W., Kagami, M. and Küpper, F.C. 2017. Integrating chytrid fungal parasites
570 into plankton ecology: research gaps and needs. Environ. Microbiol. 19(10), 3802-3822.
571 Gibson, C. 1981. Silica budgets and the ecology of planktonic diatoms in an unstratified lake
572 (Lough Neagh, N. Ireland). Int. Rev. Hydrobiol. 66(5), 641-664.
573 Gibson, C.E. and Foy, R.H. 1983. The photosynthesis and growth efficiency of a planktonic
574 blue-green alga, *Oscillatoria redekei*. Br. Phyco. J. 18(1), 39-45.
575 Goto, N., Iwata, T., Akatsuka, T., Ishikawa, M., Kihira, M., Azumi, H., Anbutsu, K. and
576 Mitamura, O. 2007. Environmental factors which influence the sink of silica in the
577 limnetic system of the large monomictic Lake Biwa and its watershed in Japan.
578 Biogeochemistry 84(3), 285-295.
579 Hampton, S.E., Galloway, A.W., Powers, S.M., Ozersky, T., Woo, K.H., Batt, R.D., Labou, S.G.,
580 O'Reilly, C.M., Sharma, S. and Lottig, N.R. 2017. Ecology under lake ice. Ecol. Lett.
581 20(1), 98-111.
582 Hannappel, S. and Strom, A. 2020. Method to determine the amount of phosphorous entering
583 Barleber See near Magdeburg via groundwater. Gewässer und Boden (in German) 13, 24-
584 30.

585 Horn, H., Paul, L., Horn, W. and Petzoldt, T. 2011. Long-term trends in the diatom composition
586 of the spring bloom of a German reservoir: is Aulacoseira subarctica favoured by warm
587 winters? Freshwat. Biol. 56(12), 2483-2499.
588 Horn, H., Paul, L., Horn, W., Uhlmann, D. and Röske, I. 2015. Climate change impeded the
589 re‐oligotrophication of the Saidenbach Reservoir. Int. Rev. Hydrobiol. 100(2), 43-60.
590 Ibelings, B.W., Gsell, A.S., Mooij, W.M., van Donk, E., van den Wyngaert, S. and Domis,
591 L.N.D. 2011. Chytrid infections and diatom spring blooms: paradoxical effects of
592 climate warming on fungal epidemics in lakes. Freshwat. Biol. 56(4), 754-766.
593 Jewson, D.H., Granin, N.G., Zhdarnov, A.A., Gorbunova, L.A. and Gnatovsky, R.Y. 2010.
594 Vertical mixing, size change and resting stage formation of the planktonic diatom
595 Aulacoseira baicalensis. Eur. J. Phycol. 45(4), 354-364.
596 Kilham, P., Kilham, S.S. and Hecky, R.E. 1986. Hypothesized resource relationships among
597 African planktonic diatoms. Limnol. Oceanogr. 31(6), 1169-1181.
598 Kirillin, G., Hochschild, J., Mironov, D., Terzhevik, A., Golosov, S. and Nützmann, G. 2011.
599 FLake-Global: Online lake model with worldwide coverage. Environ. Model. Software
600 26(5), 683-684.
601 Kirillin, G., Leppäranta, M., Terzhevik, A., Granin, N., Bernhardt, J., Engelhardt, C., Efremova,
602 T., Golosov, S., Palshin, N. and Sherstyankin, P. 2012. Physics of seasonally ice-
603 covered lakes: a review. Aquat. Sci. 74(4), 659-682.
604 Kirillin, G., Wen, L. and Shatwell, T. 2017. Seasonal thermal regime and climatic trends in
605 lakes of the Tibetan highlands. Hydrol. Earth Syst. Sci. 21(4), 1895-1909.

606 Kirilova, E.P., Bluszcz, P., Heiri, O., Cremer, H., Ohlendorf, C., Lotter, A.F. and Zolitschka, B.
607 2008. Seasonal and interannual dynamics of diatom assemblages in Sacrower See (NE
608 Germany): a sediment trap study. Hydrobiologia 614(1), 159-170.
609 Klapper, H. and Geller, W. 2001. Water quality management of mining lakes—a new field of
610 applied hydrobiology. Acta Hydrochim. Hydrobiol. 29(6-7), 363-374.
611 Kohl, J.G. and Giersdorf, K. 1991. Competition ability of two planktic diatoms under different
612 vertical light gradients, mixing-depth and -frequencies: An experimental approach.
613 Verhandlungen der Internationalen Vereinigung für Theoretische und Angewandte
614 Limnologie 24, 2652-2656.
615 Köhler, J., Hilt, S., Adrian, R., Nicklisch, A., Kozerski, H. and Walz, N. 2005. Long‐term
616 response of a shallow, moderately flushed lake to reduced external phosphorus and
617 nitrogen loading. Freshwat. Biol. 50(10), 1639-1650.
618 Köhler, J., Wang, L., Guislain, A. and Shatwell, T. 2018. Influence of vertical mixing on
619 light‐dependency of phytoplankton growth. Limnol. Oceanogr. 63(3), 1156-1167.
620 Kong, X., Zhan, Q., Boehrer, B. and Rinke, K. 2019. High frequency data provide new insights
621 into evaluating and modeling nitrogen retention in reservoirs. Water Res. 166, 115017.
622 Lampert, W., Fleckner, W., Rai, H. and Taylor, B.E. 1986. Phytoplankton control by grazing
623 zooplankton: A study on the spring clear-water phase. Limnol. Oceanogr. 31(3), 478-490.
624 Lewandowska, A.M., Striebel, M., Feudel, U., Hillebrand, H. and Sommer, U. 2015. The
625 importance of phytoplankton trait variability in spring bloom formation. ICES J. Mar. Sci.
626 72(6), 1908-1915.
627 Mironov, D. 2008. Parameterization of lakes in numerical weather prediction: description of a
628 lake model. Deutscher Wetterdienst, Offenbach am Main, Germany.

629 Mollema, P.N. and Antonellini, M. 2016. Water and (bio) chemical cycling in gravel pit lakes:
630 A review and outlook. Earth-Sci. Rev. 159, 247-270.
631 Neale, P.J., Talling, J.F., Heaney, S.I., Reynolds, C.S. and Lund, J.W. 1991. Long time series
632 from the English Lake District: Irradiance‐dependent phytoplankton dynamics during
633 the spring maximum. Limnol. Oceanogr. 36(4), 751-760.
634 Nicklisch, A. 1992. The interaction of irradiance and temperature on the growth rate of
635 *Limnothrix redekei* and its mathematical description. Arch. Hydrobiol. 63, 1-18.
636 Nicklisch, A. 1999. Competition between the cyanobacterium Limnothrix redekei and some
637 spring species of diatoms under P‐limitation. Int. Rev. Hydrobiol. 84(3), 233-241.
638 Nicklisch, A. and Kohl, J.G. 1989. The influence of light on the primary production of two
639 planktic blue-green algae. Arch. Hydrobiol. 33, 451-455.
640 Nicklisch, A., Roloff, B. and Ratsch, A. 1991. Competition experiments with two planktic blue-
641 green algae (Oscillatoriaceae). SIL Proceedings, 1922-2010 24(2), 889-892.
642 Nicklisch, A., Shatwell, T. and Kohler, J. 2008. Analysis and modelling of the interactive
643 effects of temperature and light on phytoplankton growth and relevance for the spring
644 bloom. J. Plankton Res. 30(1), 75-91.
645 Padisák, J., Scheffler, W., Kasprzak, P., Koschel, R. and Krienitz, L. 2003. Interannual
646 variability in the phytoplankton composition of Lake Stechlin (1994–2000). Arch.
647 Hydrobiol. 58, 101-133.
648 Pinheiro, J., Bates, D., DebRoy, S., Sarkar, D. and Team, R.C. 2012. nlme: Linear and
649 nonlinear mixed effects models. R package version 3(0).

650 R Core Team 2018 R: A Language and Environment for Statistical Computing, R Foundation
651 for Statistical Computing, Austria, 2015, ISBN 3-900051-07-0: URL http://www.R-
652 project.org.
653 Reavie, E.D., Cai, M., Twiss, M.R., Carrick, H.J., Davis, T.W., Johengen, T.H., Gossiaux, D.,
654 Smith, D.E., Palladino, D. and Burtner, A. 2016. Winter–spring diatom production in
655 Lake Erie is an important driver of summer hypoxia. J. Great Lakes Res. 42(3), 608-618.
656 Reynolds, C.S. (2006) The ecology of phytoplankton, Cambridge University Press.
657 Salonen, K., Leppäranta, M., Viljanen, M. and Gulati, R. 2009. Perspectives in winter
658 limnology: closing the annual cycle of freezing lakes. Aquat. Ecol. 43(3), 609-616.
659 Shatwell, T., Adrian, R. and Kirillin, G. 2016. Planktonic events may cause polymictic-dimictic
660 regime shifts in temperate lakes. Sci. Rep. 6, 24361.
661 Shatwell, T. and Köhler, J. 2019. Decreased nitrogen loading controls summer cyanobacterial
662 blooms without promoting nitrogen - fixing taxa: Long - term response of a shallow lake.
663 Limnol. Oceanogr. 64(S1), S166-S178.
664 Shatwell, T., Kohler, J. and Nicklisch, A. 2013. Temperature and photoperiod interactions with
665 silicon-limited growth and competition of two diatoms. J. Plankton Res. 35(5), 957-971.
666 Shatwell, T., Köhler, J. and Nicklisch, A. 2008. Warming promotes cold - adapted
667 phytoplankton in temperate lakes and opens a loophole for Oscillatoriales in spring.
668 Global Change Biol. 14(9), 2194-2200.
669 Shatwell, T., Köhler, J. and Nicklisch, A. 2014. Temperature and photoperiod interactions with
670 phosphorus-limited growth and competition of two diatoms. PloS One 9(7), e102367.

671 Shatwell, T., Nicklisch, A. and Köhler, J. 2012. Temperature and photoperiod effects on
672 phytoplankton growing under simulated mixed layer light fluctuations. Limnol. Oceanogr.
673 57(2), 541-553.
674 Shatwell, T., Thiery, W. and Kirillin, G. 2019. Future projections of temperature and mixing
675 regime of European temperate lakes. Hydrol. Earth Syst. Sci. 23(3), 1533-1551.
676 Siegel, D., Doney, S. and Yoder, J. 2002. The North Atlantic spring phytoplankton bloom and
677 Sverdrup's critical depth hypothesis. Science 296(5568), 730-733.
678 Soetaert, K.E., Petzoldt, T. and Setzer, R.W. 2010. Solving differential equations in R: package
679 deSolve. J. Stat. Softw. 33(9), 1-25.
680 Sommer, U., Adrian, R., De Senerpont Domis, L., Elser, J.J., Gaedke, U., Ibelings, B., Jeppesen,
681 E., Lürling, M., Molinero, J.C. and Mooij, W.M. 2012. Beyond the Plankton Ecology
682 Group (PEG) model: mechanisms driving plankton succession. Annu. Rev. Ecol. Evol.
683 Syst. 43, 429-448.
684 Sommer, U., Gliwicz, Z.M., Lampert, W. and Duncan, A. 1986. The PEG-model of seasonal
685 succession of planktonic events in fresh waters. Arch. Hydrobiol. 106(4), 433-471.
686 Sommer, U. and Lengfellner, K. 2008. Climate change and the timing, magnitude, and
687 composition of the phytoplankton spring bloom. Global Change Biol. 14(6), 1199-1208.
688 Sorvari, S., Korhola, A. and Thompson, R. 2002. Lake diatom response to recent Arctic
689 warming in Finnish Lapland. Global Change Biol. 8(2), 171-181.
690 Spaulding, S. and Baron, J. 1993. Winter phytoplankton dynamics in a subalpine lake, Colorado,
691 USA. Arch. Hydrobiol., 179-198.
692 Sverdrup, H. 1953. On conditions for the vernal blooming of phytoplankton. ICES J. Mar. Sci.
693 18(3), 287-295.

694 Tabata, S. 1973. A simple but accurate formula for the saturation vapor pressure over liquid
695 water. J. Appl. Meteorol. 12(8), 1410-1411.
696 Talling, J. 1957. Photosynthetic characteristics of some freshwater plankton diatoms in relation
697 to underwater radiation. New Phytol. 56(1), 29-50.
698 Thackeray, S., Jones, I. and Maberly, S. 2008. Long‐term change in the phenology of spring
699 phytoplankton: species‐specific responses to nutrient enrichment and climatic change. J.
700 Ecol. 96(3), 523-535.
701 Thackeray, S.J., Henrys, P.A., Hemming, D., Bell, J.R., Botham, M.S., Burthe, S., Helaouet, P.,
702 Johns, D.G., Jones, I.D. and Leech, D.I. 2016. Phenological sensitivity to climate across
703 taxa and trophic levels. Nature 535(7611), 241.
704 Thiery, W., Martynov, A., Darchambeau, F., Descy, J.P., Plisnier, P.D., Sushama, L. and Van
705 Lipzig, N.P.M. 2014. Understanding the performance of the FLake model over two
706 African Great Lakes. Geosci. Model Dev. 7(1), 317-337.
707 Townsend, D.W., Keller, M.D., Sieracki, M.E. and Ackleson, S.G. 1992. Spring phytoplankton
708 blooms in the absence of vertical water column stratification. Nature 360, 59-62.
709 Vincent, W.F. 1983. Phytoplankton production and winter mixing: contrasting effects in two
710 oligotrophic lakes. J. Ecol. 71, 1-20.
711 Wentzky, V.C., Frassl, M.A., Rinke, K. and Boehrer, B. 2019. Metalimnetic oxygen minimum
712 and the presence of Planktothrix rubescens in a low-nutrient drinking water reservoir.
713 Water Res. 148, 208-218.
714 Wilhelm, S.W., LeCleir, G.R., Bullerjahn, G.S., McKay, R.M., Saxton, M.A., Twiss, M.R. and
715 Bourbonniere, R.A. 2014. Seasonal changes in microbial community structure and

716 activity imply winter production is linked to summer hypoxia in a large lake. FEMS
717 Microbiol. Ecol. 87(2), 475-485.
718 Winder, M., Reuter, J.E. and Schladow, S.G. 2008. Lake warming favours small-sized
719 planktonic diatom species. P. Roy. Soc. B-Biol. Sci. 276(1656), 427-435.
720 Winder, M. and Schindler, D.E. 2004. Climate change uncouples trophic interactions in an
721 aquatic ecosystem. Ecology 85(8), 2100-2106.
722 Winslow, L., Read, J., Woolway, R., Brentrup, J., Leach, T., Zwart, J., Albers, S. and Collinge,
723 D. 2019 rLakeAnalyzer: Lake Physics Tools. R package version 1.11.4.1.
724 https://CRAN.R-project.org/package=rLakeAnalyzer.
725 Woolway, R.I. and Merchant, C.J. 2019. Worldwide alteration of lake mixing regimes in
726 response to climate change. Nat. Geosci. 12(4), 271-276.
727 Xiao, W., Huang, Y., Mi, W., Wu, H. and Bi, Y. 2019. Variation of diatoms and silicon in a
728 tributary of the three gorges reservoir: Evidence of interaction. Water 11(7), 1369.
729 Yang, Y., Stenger-Kovács, C., Padisák, J. and Pettersson, K. 2016. Effects of winter severity on
730 spring phytoplankton development in a temperate lake (Lake Erken, Sweden).
731 Hydrobiologia 780(1), 47-57.

732

Figure and Table captions

Figure 1. Location and bathymetry map of Lake Barleber in central Germany and two sampling sites (BA1 and BAM). The scale bar refers only to the bathymetry map of the lake (For interpretation of the references to colour in this figure legend, the reader is referred to the Web version of this article).

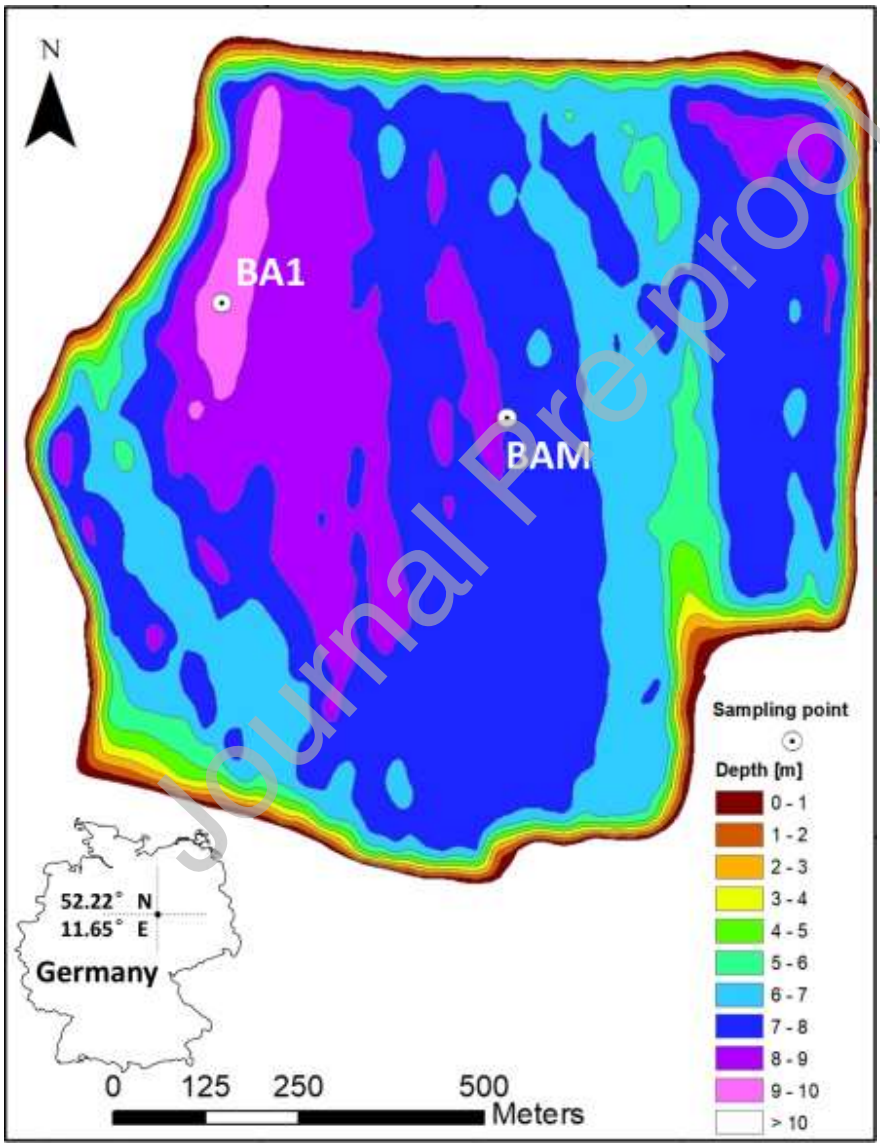

739 **Figure 2.** Conceptual diagram of the ecological model to simulate lake phytoplankton dynamics
740 in winter. P and P_{sed} represent the dissolved phosphorus in water and stored in sediment pore
741 water, respectively, and the same for silicon (Si and Si_{sed}) (For interpretation of the references to
742 colour in this figure legend, the reader is referred to the Web version of this article).

743

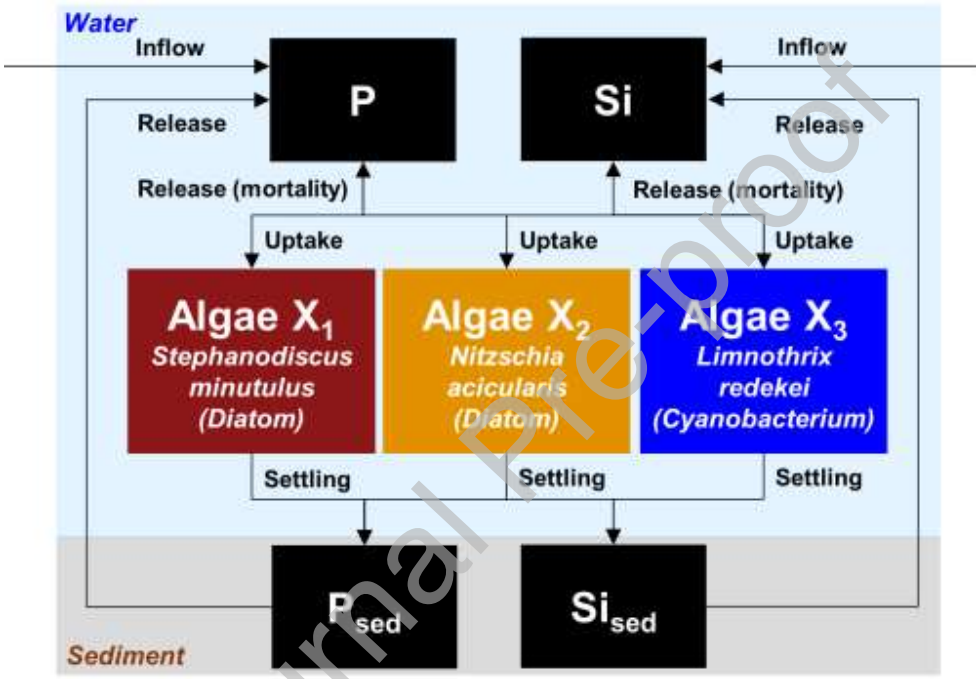

744

745 **Figure 3. (a)** Dynamics of the phytoplankton community in surface water of Lake Barleber
746 measured using a multi-channel fluorescence probe (PhycoProbe; BBE Moldaenke GmbH,
747 Schwentinetal, Germany). The biomass of the different groups of phytoplankton is given as
748 chlorophyll-a concentrations aggregated to daily averages. The period of the diatom bloom is
749 highlighted by orange shading. **(b and c)** High frequency water temperature profiles from the
750 chain sensors at 15-min intervals. The periods of stratification, ice cover and recirculation are
751 labeled by colour bars on the bottom. The period of ice cover is presented with more details (For

752 interpretation of the references to colour in this figure legend, the reader is referred to the web
753 version of this article).

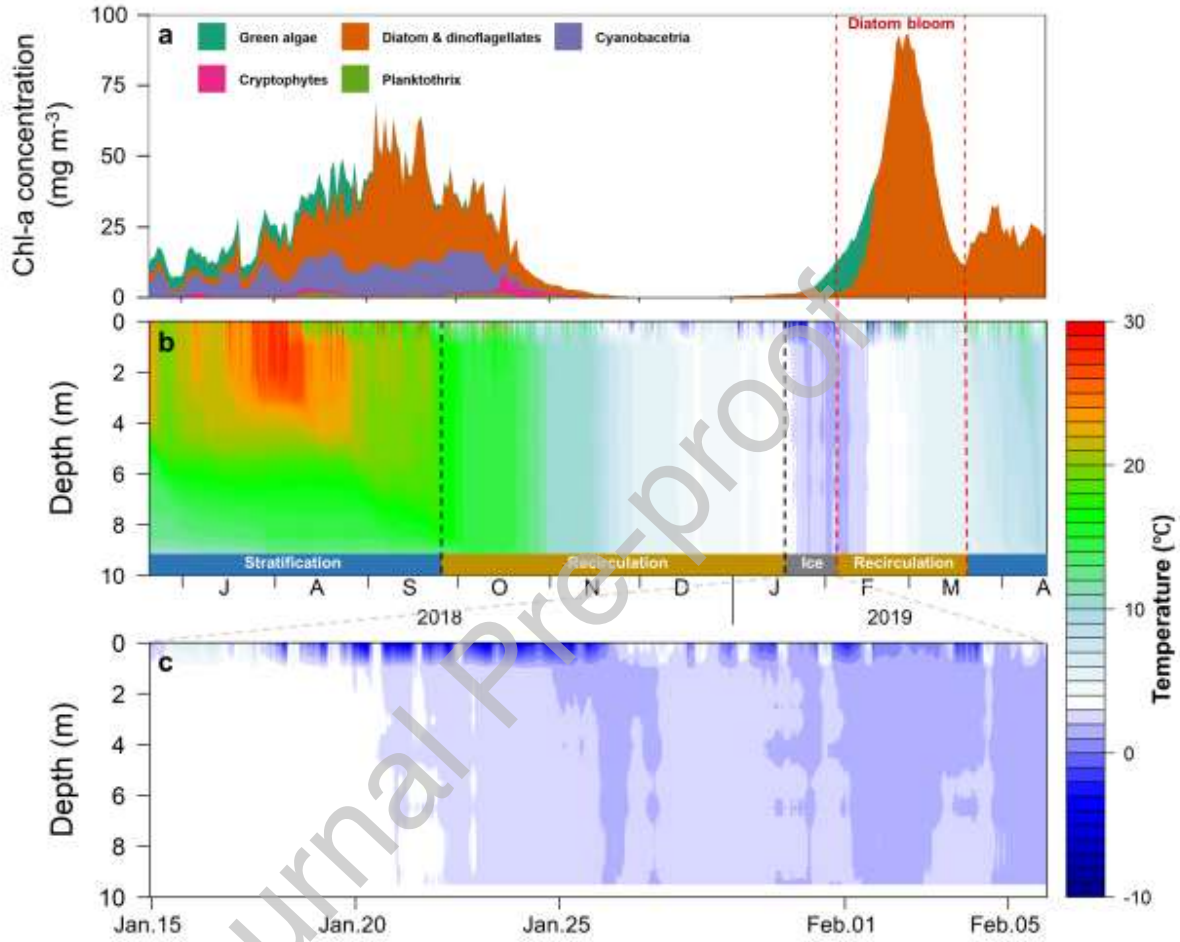

754

755 **Figure 4**. Diatom dynamics and lake physical conditions during January 15th - February 15th,
756 2019. **(a)** Chl-a concentration of diatom (mg·L^{-1}) aggregated to daily resolution (in logarithmic
757 scale), where the periods of ice cover and the diatom bloom are highlighted by shading. **(b)** Air
758 (from DWD) and water (from thermistor chain) temperature (°C) at various depths at hourly
759 intervals. **(c)** The occurrence of snow (from DWD) and the modeled ice thickness (cm) by FLake.
760 **(d)** Global radiation (mol·m^{-2}·d^{-1}, from DWD), calculated mean underwater light intensity in the

761 mixed layer ($mol \cdot m^{-2} \cdot d^{-1}$) and effective photoperiod (h), based on calculated light attenuation
762 coefficient from Secchi depth. The dashed blue line represents the correction during ice cover
763 (50% reduction). The horizontal dashed red lines show the critical light intensity for positive net
764 growth of phytoplankton (1.3 with a range of 0.8-2.5 $mol \cdot m^{-2} \cdot d^{-1}$) (For interpretation of the
765 references to colour in this figure legend, the reader is referred to the web version of this article).

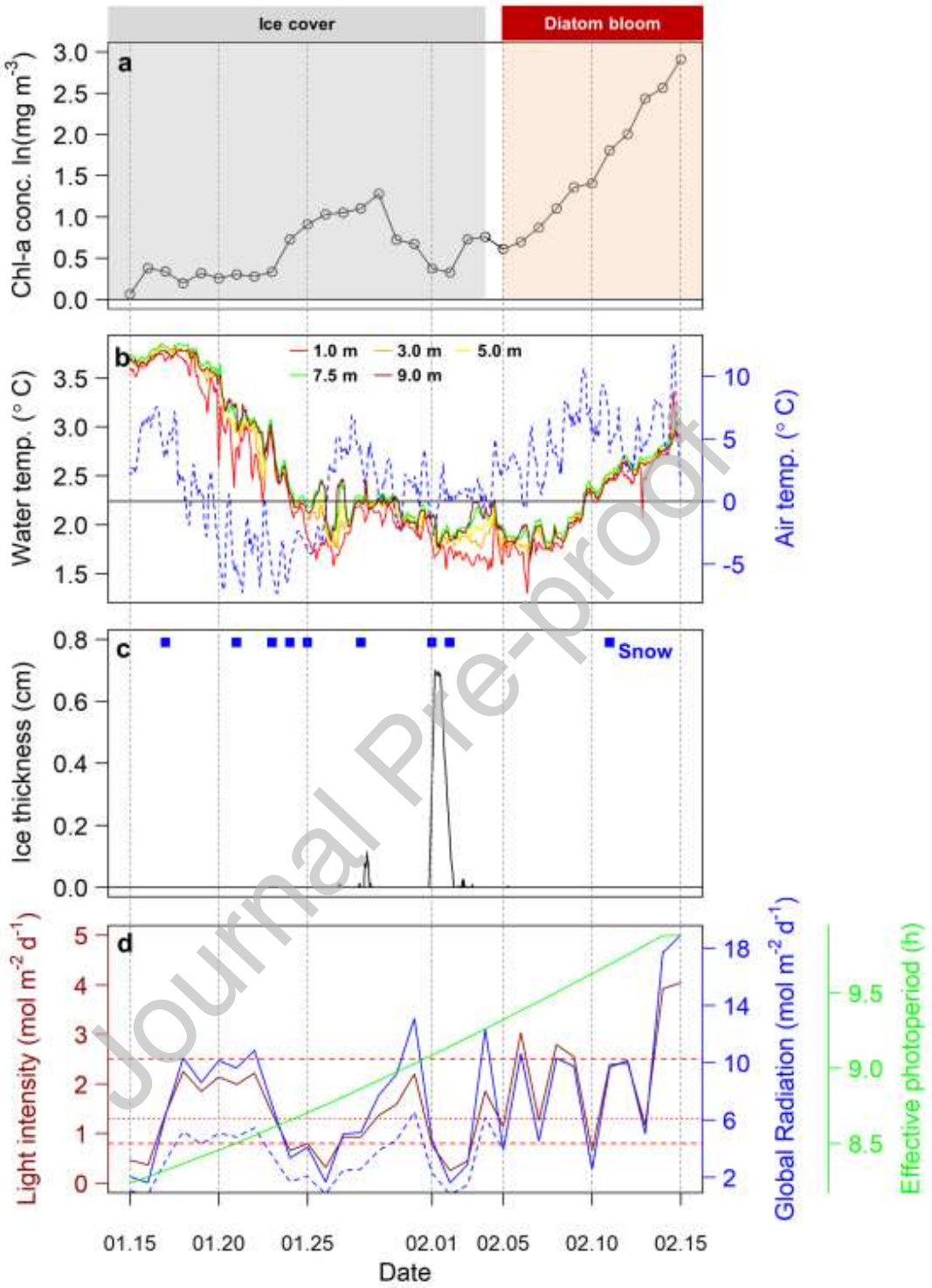

766

767 **Figure 5**. Comparison of modeled (Mod) data from the ecological model and observed (Obs)

768 data for various water quality variables during January 1st to March 31st, 2019. Note that for Chl-

769 a, the observed data represent the measurement by a BBE probe in surface water, while those for
770 TP, SRP and Si concentrations are the volume-weighted values of the whole water column.
771 ***RMSE***: root mean-square error, ***r***: correlation coefficient, and ***n***: sample size.

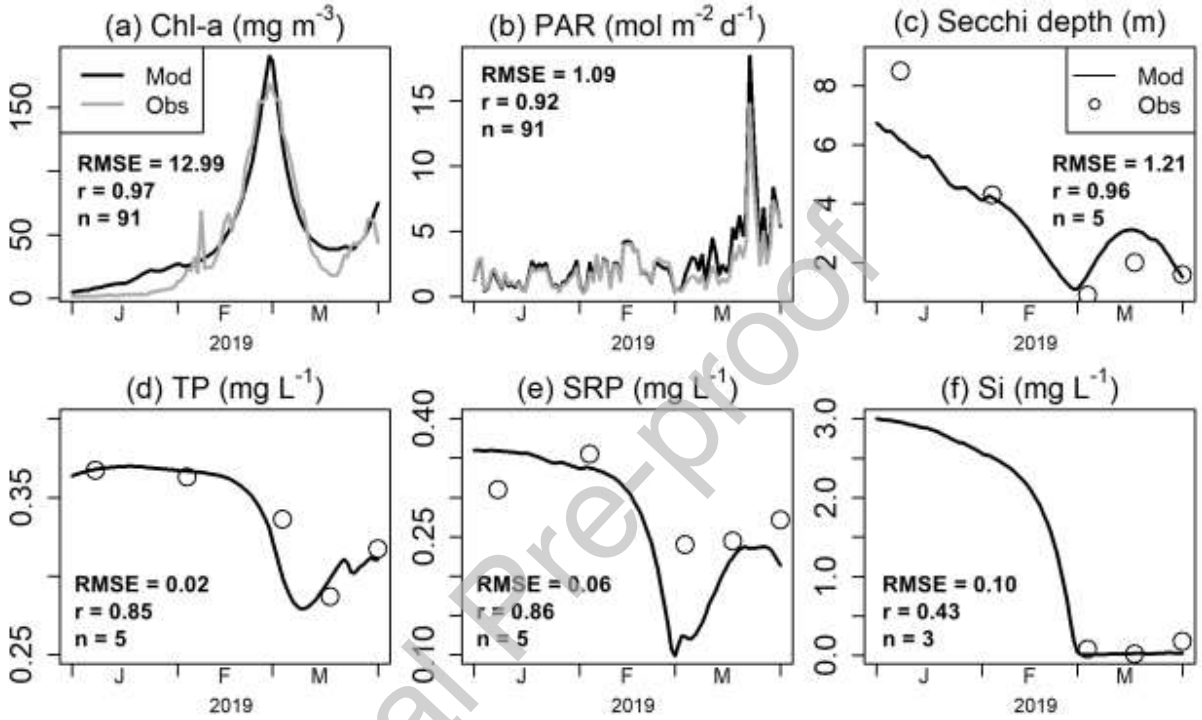

772

773 **Figure 6.** Ecological model outputs during January 1st to March 31st, 2019. **(a)** biomass (in
774 biovolume, $mm^3 \cdot m^{-3}$) variations of three modeled phytoplankton species; **(b)** modeled net
775 growth rate (d^{-1}) of *S. minutulus* under additional constraints by temperature (red), temperature +
776 photoperiod (orange), temperature + photoperiod + mean light intensity (blue), and finally the
777 cumulative effect of adding nutrients (phosphorus and silicon, black). The net growth rate
778 represents the ultimate change rate of algal biomass including the processes of growth,
779 respiration, mortality, and settling. The inner panel shows the limitations of phosphorus and
780 silicon. The period of the winter diatom bloom is highlighted by an orange shade in both panels.
781 The constraint index (colour bar at bottom left) shows the major constraint by either light or

782 temperature on the growth of *S. minutulus* before the peak of the bloom (when nutrient limitation
783 became relevant), which is determined by the algorithm demonstrated in Fig. 7 (For
784 interpretation of the references to colour in this figure legend, the reader is referred to the web
785 version of this article).

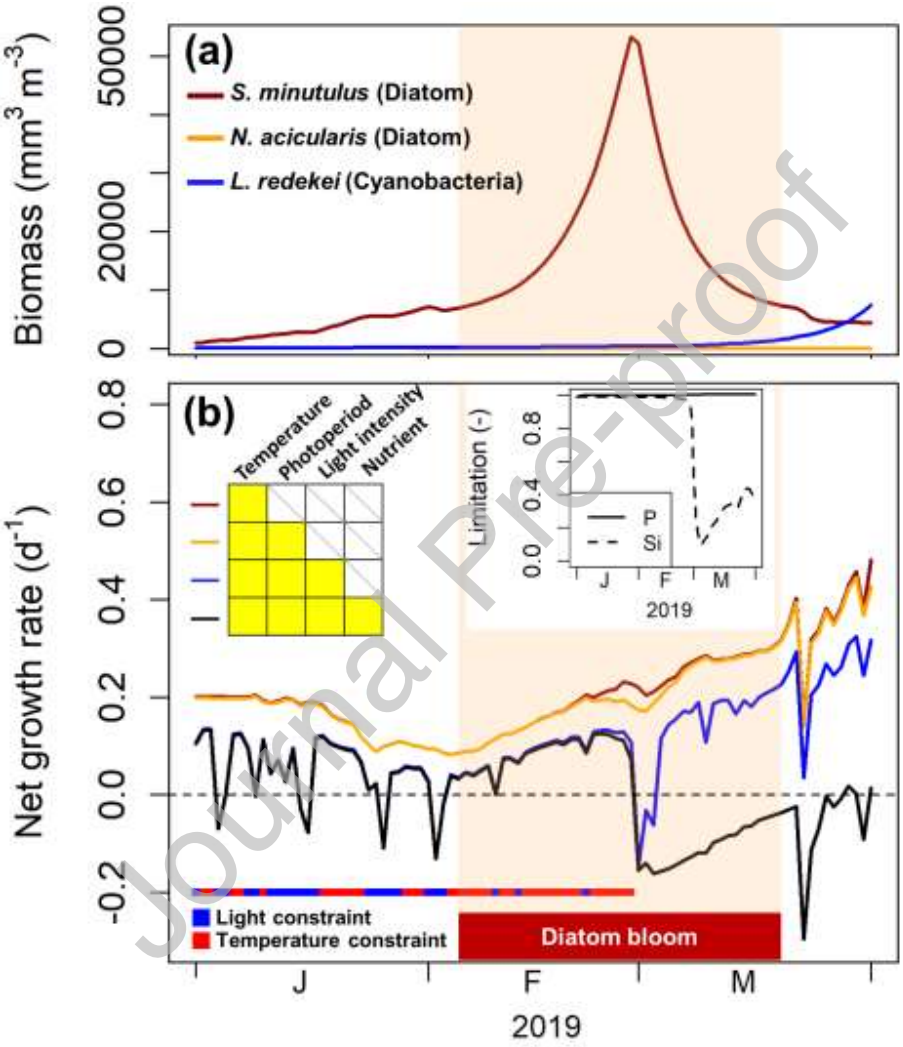

786 **Figure 7.** Model
787 evaluations on the interactive effects of water temperature and light on diatom growth before and
788 during the bloom. **(a)** The isoclines (curved lines) of constant specific growth rate (μ) at 0.2 d^{-1}
789 for the three modeled species, together with daily mean water temperature (T) and light intensity
790 (I) in the water column during January 1st and March 20th, 2019 in Lake Barleber (circles).

Circles with red border correspond to the period of the diatom bloom (Feb. 5th to Mar. 20th), while circles with blue border represents the period before the bloom. The curved regions of the isoclines show where light-temperature interactions (co-constraint of growth) are strongest. Points near the horizontal limbs of the isoclines show conditions where temperature is more constraining, and points near the vertical limbs show where light is more constraining. **(b)** Relative strength of constraint by light and temperature on the growth of *S. minutulus*. The points are the same as in panel (a) and the arrows represent the scaled gradient vector $\left(\frac{\partial \mu}{\partial I}, \frac{\partial \mu}{\partial T}\right)$, showing the relative increase in μ in response to an incremental increase in both water temperature and light. The first term in the vector (horizontal component) is equivalent to the instantaneous light constraint, and the second (vertical component) to the instantaneous temperature constraint. Note that both water temperature and light during this period are rescaled to the range of [0, 1]. The red dashed curve represents the condition where light and temperature pose the same strength of constraint to the growth. The curve therefore divides the field into two parts demonstrating light-constraint dominant (upper) and temperature-constraint dominant (below). **(c-e)** Contour plot subpanels with isoclines show the values under different temperature (T) and light (I) conditions for *S. minutulus*, as follows: **(c)** specific growth rate (μ); **(d)** partial derivative $\left(\frac{\partial \mu}{\partial I}\right)$; and **(e)** partial derivative $\left(\frac{\partial \mu}{\partial T}\right)$ (For interpretation of the references to colour in this figure legend, the reader is referred to the web version of this article).

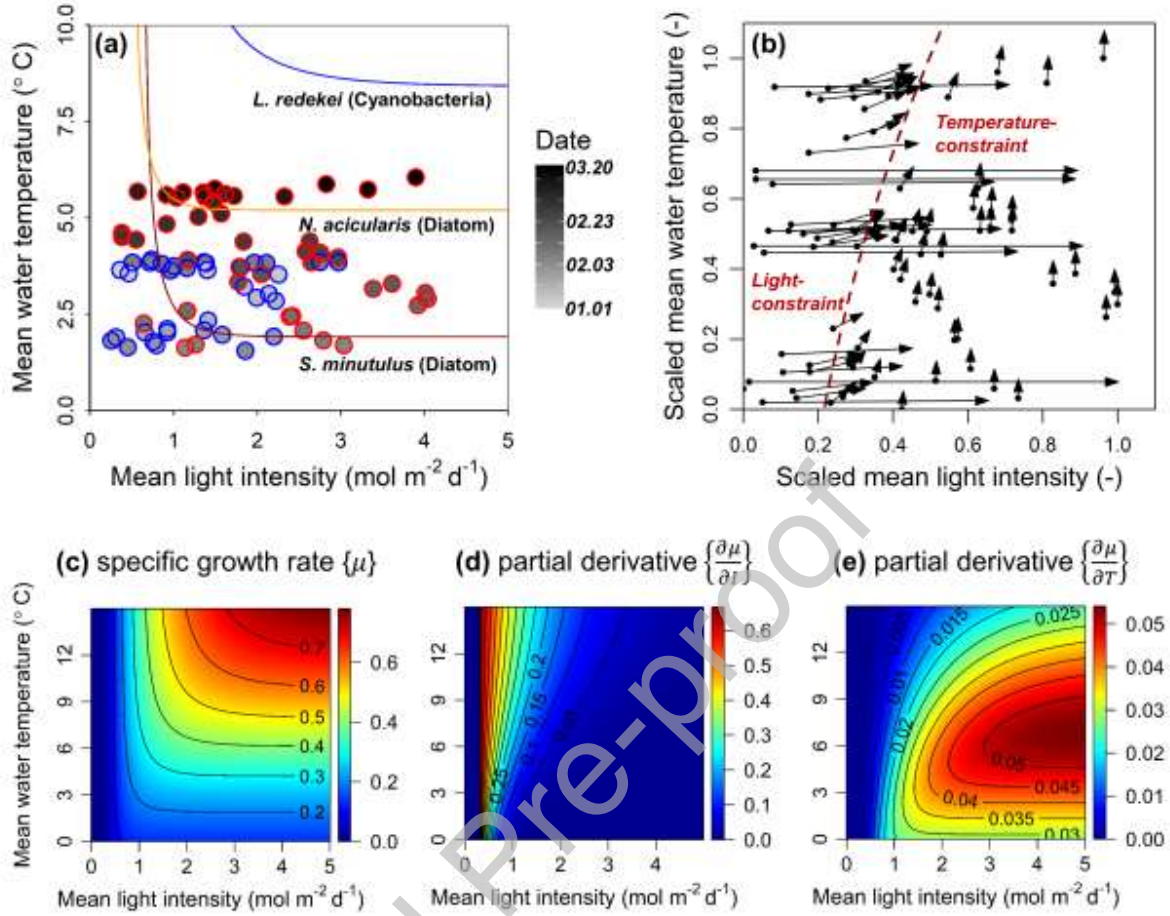

809

810 **Table 1.** Mean (±SE) nutrient concentrations (volume-weighted) in Lake Barleber from
811 October 2018 to March 2019 (circulation period) before and after the onset of the winter diatom
812 bloom, and statistical analysis for testing the differences using generalized least squares (GLS)
813 model with first-order autoregressive process (AR(1)) (* $p < 0.05$, ** $p < 0.01$, *** $p < 0.001$).
814 NO_3-N concentrations before January 2019 were not included in the analysis.

Water quality variable	before bloom	after bloom	p-value	t-value
TP (µg·L^{-1})	366±4.8	311±24.5	0.0093**	-3.77
SRP (µg·L^{-1})	337±7.5	242±2.3	0.0005***	-6.91
TN (mg·L^{-1})	2.44±0.19	1.55±0.14	0.0435*	-2.55
NH_4-N (mg·L^{-1})	0.76±0.07	0.17±0.08	0.0048**	-4.35

NO_3-N (mg·L^{-1})	0.45±0.06	0.29±0.03	0.1293	-2.50
Si (mg·L^{-1})	1.55±0.07	0.05±0.03	0.0028**	-18.90

815

816 GA

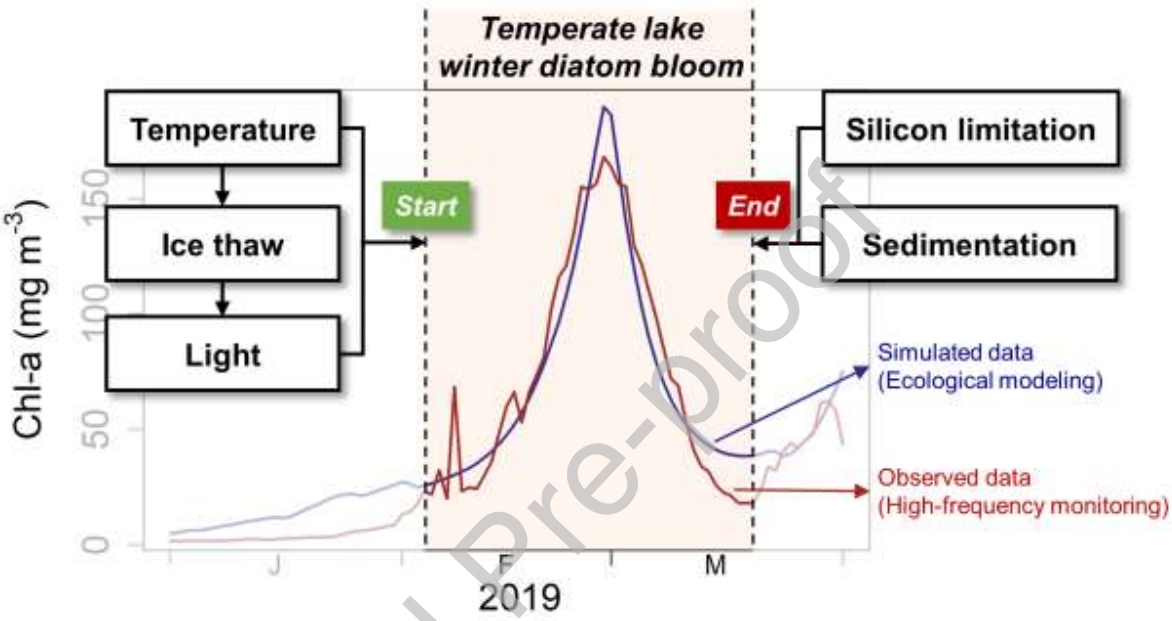

817

818

819 **Declaration of interests**

820

821 ☒ The authors declare that they have no known competing financial interests or personal
822 relationships that could have appeared to influence the work reported in this paper.

823